























RESEARCH ARTICLE | MAY 06 2024

Achieving stationary high performance plasmas at Wendelstein 7-X


Special Collection: [Proceedings of PLASMA 2023 - International Conference on Research and Applications of Plasmas](#)

A. Langenberg  ; F. Warmer ; G. Fuchert ; O. Ford ; S. Bozhenkov ; T. Andreeva ; S. Lazerson ; N. A. Pablant ; T. Gonda ; M. N. A. Beurskens ; K.-J. Brunner ; B. Buttenschön ; A. Dinklage ; D. Hartmann ; J. Knauer ; O. Marchuk ; E. Pasch; F. Reimold ; T. Stange ; Th. Wegner ; O. Grulke ; R. C. Wolf ; W7-X Team



Phys. Plasmas 31, 052502 (2024)


<https://doi.org/10.1063/5.0199958>



APL Machine Learning

2023 Papers with Best Practices in Data Sharing and Comprehensive Background

[Read Now](#)



Achieving stationary high performance plasmas at Wendelstein 7-X

Cite as: Phys. Plasmas **31**, 052502 (2024); doi: [10.1063/5.0199958](https://doi.org/10.1063/5.0199958)

Submitted: 24 January 2024 · Accepted: 14 April 2024 ·

Published Online: 6 May 2024



View Online



Export Citation



CrossMark

A. Langenberg,^{1,a)} F. Warmer,^{1,2} G. Fuchert,¹ O. Ford,¹ S. Bozhenkov,¹ T. Andreeva,¹ S. Lazerson,¹ N. A. Pablant,³ T. Gonda,³ M. N. A. Beurskens,¹ K.-J. Brunner,¹ B. Buttenschön,¹ A. Dinklage,¹ D. Hartmann,¹ J. Knauer,¹ O. Marchuk,⁴ E. Pasch,¹ F. Reimold,¹ T. Stange,¹ Th. Wegner,¹ O. Grulke,^{1,5} R. C. Wolf,^{1,6} and W7-X Team^{b)}

AFFILIATIONS

¹Max-Planck-Institut für Plasmaphysik, 17491 Greifswald, Germany

²Eindhoven University of Technology, 5600 Eindhoven, Netherlands

³Princeton Plasma Physics Laboratory, Princeton, New Jersey 08543, USA

⁴Forschungszentrum Jülich GmbH, Institut für Energie- und Klimaforschung, 52425 Jülich, Germany

⁵Technical University of Denmark, 2800 Kongens Lyngby, Denmark

⁶Technische Universität Berlin, 10623 Berlin, Germany

Note: This paper is part of the Special Topic, Proceedings of PLASMA 2023 - International Conference on Research and Applications of Plasmas.

^{a)}Author to whom correspondence should be addressed: andreas.langenberg@ipp.mpg.de

^{b)}Thomas Sunn Pedersen et al., Nucl. Fusion **62**, 042022 (2022).

ABSTRACT

This work reports on recent results on the search for high performance plasma scenarios at the magnetically confined stellarator fusion device Wendelstein 7-X. In four new designed scenarios, the development from transient toward stationary plasmas of improved performance has been realized. In particular, a high performance duration of up to 5 s, an energy confinement time of 0.3 s, a diamagnetic energy of 1.1 MJ, a central ion temperature of 2.2 keV, and a fusion triple product of $3.4 \times 10^{19} \text{ m}^{-3} \cdot \text{keV} \cdot \text{s}$ have been achieved, and previously observed limitations of the machine have been overcome, regarding both the performance and its duration. The two main experimental techniques for stationary high performance are neutral beam injection core fueling on the one hand and the use of a magnetic field configuration with internal islands on the other hand. Two of the developed scenarios are expected to be extendable straightforward toward a duration of several tens of seconds, making use of the long pulse operation capabilities of W7-X.

© 2024 Author(s). All article content, except where otherwise noted, is licensed under a Creative Commons Attribution (CC BY) license (<https://creativecommons.org/licenses/by/4.0/>). <https://doi.org/10.1063/5.0199958>

I. INTRODUCTION

The development of high performance (HP) plasma scenarios, in particular with respect to a maximization of the fusion triple product $n_e T_i \tau_E$ under steady-state plasma conditions,¹ is one of the main important and also most challenging goals of the magnetically confined fusion device Wendelstein 7-X (W7-X).² Despite significant achievements like the proof of neoclassical optimization,³ a transient high fusion triple product,⁴ or steady-state plasma conditions with complete detachment,^{5,6} the majority of W7-X plasma scenarios were dominated by turbulent transport mechanisms,⁷ limiting the plasma performance as evident from energy^{8–10} as well as impurity transport studies.^{11–17} As a result, a saturation of the ion temperature $T_i \leq 1.7$

keV,¹⁸ limited energy confinement times $\tau_E \approx 0.2$ s, and fusion triple products $n_e T_i \tau_E \leq 0.3 \times 10^{20} \text{ m}^{-3} \cdot \text{keV} \cdot \text{s}$ were observed in standard gas fueled plasmas.⁴ Consequently, within this work, high performance is defined as a plasma scenario passing one or more of the following limitations:

- Overcome of the T_i limit with $T_i \geq 1.7$ keV;
- ISS04 scaling with $\tau_E / \tau_{ISS04} \geq 0.7$;
- A fusion product of $n_e T_i \tau_E \geq 0.3 \times 10^{20} \text{ m}^{-3} \cdot \text{keV} \cdot \text{s}$.

As τ_E has well known dependencies of several plasma parameters, here τ_E is related to the ISS04 scaling¹⁹ (see Sec. III for details) with a limiting ratio of $\tau_E / \tau_{ISS04} = 0.7$ that has not been exceeded in gas

fueled plasmas²⁰ at higher plasma densities of $n_e > 5 \times 10^{19} \text{ m}^{-3}$. Similarly, $n_e T_i \tau_E = 0.3 \times 10^{20} \text{ m}^{-3} \cdot \text{keV} \cdot \text{s}$ has been observed as a limit for the fusion product⁴ in turbulence dominated plasmas of W7-X.

Fortunately, the use of alternative fueling schemes like cryogenic ice pellet fueling,²¹ neutral beam fueling,²² and perturbative impurity injections²³ showed a reduction of turbulent transport with significantly improved performance beyond the above-mentioned limitations, although, only for short term, transient phases on the order of ~ 200 ms.

In this paper, results on the transition from transient toward steady-state high performance plasma scenarios will be presented, making use of combined neutral beam injection²² (NBI) and electron cyclotron resonance²⁴ (ECR) heating schemes, wall conditioning,^{25,26} and magnetic field scan techniques.^{27,28}

Section II introduces four new developed high performance scenarios and its main plasma parameters, followed by a discussion on the performance of each scenario with respect to its energy confinement and fusion triple product in Sec. III, and implications for future scenario developments discussed in Sec. IV.

II. EXPERIMENT SCENARIO DEVELOPMENT

W7-X plasmas are generated by the two main heating sources, ECR and NBI heating, providing powers of up to $P_{ECRH} = 7.5 \text{ MW}$ and $P_{NBI} = 4.0 \text{ MW}$, respectively, to the plasma that itself has a volume of 30 m^3 . The plasma density is set via several fast piezo gas valves⁵ that are feedback controlled on the line of sight averaged electron density n_e measured by the interferometer diagnostic.²⁹ The diamagnetic energy W_{dia} , the central ion temperature T_i , and electron density profiles of the plasma are measured by the Rogowski coils,³⁰ the x-ray imaging crystal spectrometers,³¹ and the Thomson scattering system.³²

In the following paragraphs, the temporal evolution of those main plasma parameters will be discussed in detail for four dedicated hydrogen plasma scenarios of notably improved performance.

A. Scenario 1: Steady NBI+ECR heating

Scenario 1 was initially conducted as a test scenario for steady NBI heating of $P_{NBI} = 3.0 \text{ MW}$, assisted with $P_{ECRH} = 1.9 \text{ MW}$ for plasma startup at medium density $n_e = 0.4 \times 10^{20} \text{ m}^{-3}$ as shown on the left of Fig. 1.

Remarkably, the combination of $P_{NBI} > P_{ECRH}$ allowed to push T_i above its saturation limit. This limit used to clamp central ion temperatures of W7-X in previous campaigns to $T_i \leq 1.7 \text{ keV}$ as a consequence of enhanced ion temperature gradient (ITG) turbulence for increased T_e/T_i ratios.¹⁸ In fact, within the entire duration of the NBI heating phase, the T_i limit (dashed line in Fig. 1) could be exceeded significantly, reaching $T_i = 2.1 \text{ keV}$ and $W_{dia} = 0.45 \text{ MJ}$ for 5 s. This is the first time a steady-state scenario of $T_i > 1.7 \text{ keV}$ has been realized at W7-X, only limited by the duration of the NBI heating phase. At the end of NBI heating at $t = 6 \text{ s}$, T_i falls back to its saturation limit in timescales of the energy confinement time of $\tau_E = 100 \text{ ms}$, see also Fig. 5.

Figure 2 on the left shows the electron density profiles of Scenario 1 in the limited (blue line) and improved performance phase (orange line), and the latter one being increased due to the NBI fueling effect. As previously observed for plasmas of improved performance,^{4,7} also the n_e profile of Scenario 1 shows a slightly steeper edge density gradient in the improved performance phase compared to the limited performance phase as indicated by the dashed lines marking the n_e gradients at $\rho = 0.9$. Note that in the same experiment program, a similar profile shaping with an increased edge density gradient in the n_e profile (not shown) has been induced by an external gas puff from

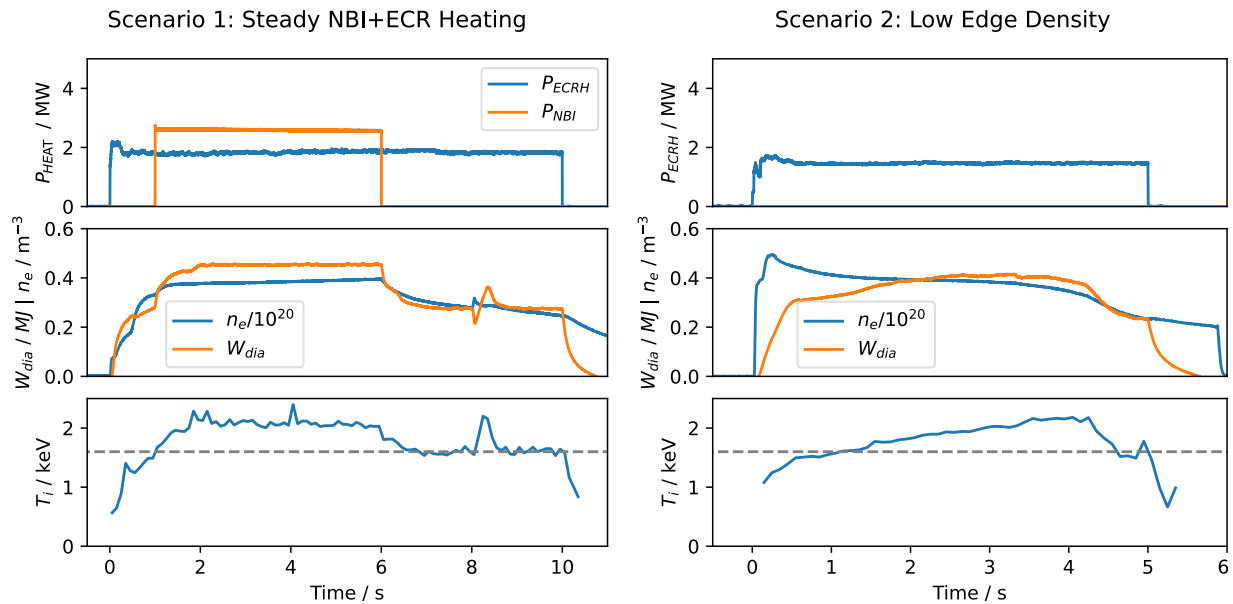


FIG. 1. Time traces of ECR and NBI heating power (upper panels), the diamagnetic energy and averaged electron density (middle panels), and central ion temperature (lower panels) for the W7-X programs 20221207.054 (left) and 20221123.003 (right). The dashed horizontal lines represent the T_i saturation limit.

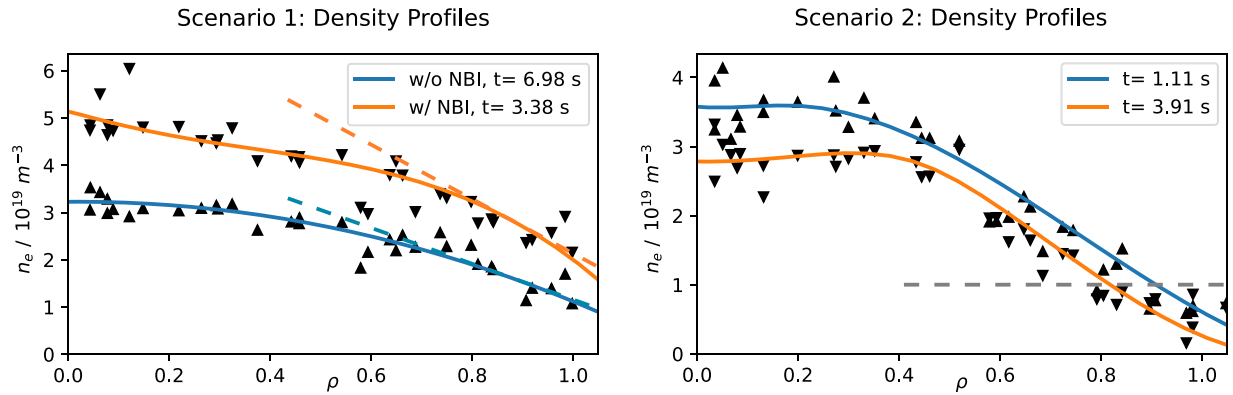


FIG. 2. Left: Electron density profiles for Scenario 1 in the improved (orange) vs limited (blue) performance phases. Dashed lines indicate edge density gradients being higher in the case of improved performance. Right: Electron density profiles for Scenario 2 at the beginning (blue) and the end (orange) of the high performance phase. The horizontal dashed line marks the unusual low edge density values of $n_e < 1.0 \times 10^{19} \text{ m}^{-3}$ for $\rho > 0.8$.

the gas puff imaging diagnostic at $t = 8.0$ s, yielding a similar but transient increase in T_i for about 300 ms, see lower left of Fig. 1 for $8.0 \leq t \leq 8.5$ s.

The steady-state character of Scenario 1 during the NBI phase is highly beneficial for achieving T_i above the saturation limit, and the absolute diamagnetic energy, however, is comparably low. The realization of higher diamagnetic energies with breaking of the T_i saturation and a more detailed discussion on effects of the $P_{\text{NBI}}/P_{\text{ECRH}}$ ratio on the plasma performance and the n_e profile peaking are given in paragraph D for Scenario 4.

B. Scenario 2: Low edge density

Scenario 2 has been conducted directly after a fresh boronization³³ of the first wall with $P_{\text{ECRH}} = 1.6$ MW at an averaged electron density of $n_e = 0.4 \times 10^{20} \text{ m}^{-3}$, as shown in Fig. 1 on the right. For a direct comparison, the left and right ordinates in Fig. 1 are shown on the same scales. Although Scenario 2 has compared to Scenario 1 slightly less ECRH power, no additional NBI heating phase, and the same averaged electron density, it also shows improved performance. Especially, the energy confinement time of $\tau_E = 300$ ms is significantly increased, and also the central ion temperature is above the saturation limit with a maximum value of $T_i = 2.2$ keV. However, T_i and W_{dia} are not stationary but do both slowly rise with slightly decreasing n_e until $t = 4.2$ s, when an unknown event ended the improved performance phase.

The density profiles of Scenario 2 shown in Fig. 2 on the right exhibit a particular low edge density of $n_e < 1 \times 10^{19} \text{ m}^{-3}$ for $\rho > 0.8$, see dashed line in Fig. 2. Moreover, the n_e profiles have a pronounced and radially extended density gradient ranging from the plasma edge toward the bulk plasma from $\rho = 1.0$ up to 0.4. This combination of low edge density yielding the radially extended density gradient is thought to be responsible for the improved performance. For a conclusive analysis however, additional experimental data are required and are planned to be conducted in the upcoming operational phase of W7-X.

In addition to the non-stationary character of Scenario 2, its application also for higher ECR heating powers $P_{\text{ECRH}} > 1.6$ MW as well as the required wall conditioning state needs to be clarified

experimentally in more detail, in particular with respect to a feasible scaling toward high density operation.

C. Scenario 3: Internal islands configuration

Scenario 3 has been developed within a series of experiment programs, scanning the iota profile of the W7-X magnetic configurations with respect to an optimized performance. As a result of this scan, the magnetic configuration FMM002²⁷ was identified, yielding a particular high diamagnetic energy W_{dia} , as shown in Fig. 3, left. With pure ECR heating of $P_{\text{ECRH}} = 4.0$ MW at a high density of $n_e = 9.0 \times 10^{19} \text{ m}^{-3}$, a diamagnetic energy of $W_{\text{dia}} = 0.8$ MJ has been achieved in steady-state for a duration of 5 s, see Fig. 3, left. In fact, as the plasma parameters are entirely stationary after reaching the final density level for $5 \leq t \leq 10$ s, the duration of the high performance phase is only limited by the length of ECR heating, which, in principle, is designed to operate for up to 30 min. Compared to the W7-X magnetic standard configuration, the iota optimized W_{dia} is enhanced by 10%–15%. The reason for this enhancement is not clarified yet and under discussion. Initial results show optimal performance in case the iota profile is crossing rationals at a radial position close to the last closed flux surface²⁷ on the one hand and a stabilizing effect of the radial electric field on density fluctuations and ion turbulent gradient driven instabilities³⁴ on the other hand.

The edge density gradient is again enhanced in the high performance phase and reduced in the low performance phase, similar to Scenario 1, as indicated by the dashed lines shown on the left of Fig. 4.

Despite the high performance with respect to W_{dia} and the steady-state character of Scenario 3, it suffers from the saturation of T_i not exceeding $T_i > 1.7$ keV, see dashed line on the left of Fig. 3. This limit, however, will be overcome in Scenario 4, also using the magnetic configuration FMM002, but a different density fueling technique.

D. Scenario 4: Controlled density peaking

In Scenario 4, an advanced heating scheme, using single and combined sequences of NBI and ECR heating, has been developed as shown in Fig. 3 on the top right. In the beginning, a sequence of 1 s with pure ECR heating for plasma startup at medium density is

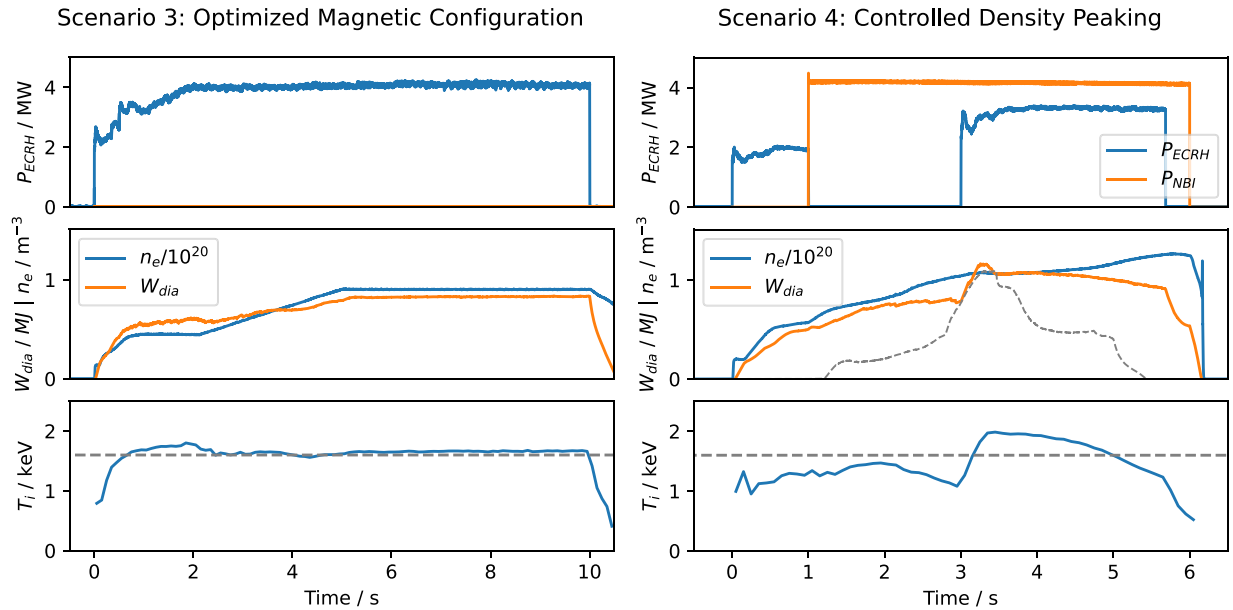


FIG. 3. Time traces of ECR and NBI heating power (upper panels), the diamagnetic energy and averaged electron density (middle panels), and central ion temperature (lower panels) for the W7-X programs 20230216.059 (left) and 20230216.063 (right). Dashed horizontal lines represent the T_i saturation limit, and the dashed gray line in the right middle panel corresponds to the W_{dia} time trace of the transient high performance program after pellet injections.⁴

followed by a pure NBI heating phase further rising the electron density. Finally, a combined NBI and ECR heating phase at $t > 3$ s maximizes the combined heating power to $P_{ECRH} + P_{NBI} = 7.6$ MW (see Table I) at high density. Within this heating scenario, the highest diamagnetic energy of all four scenarios has been achieved with $W_{dia} = 1.1$ MJ, as shown in the middle right panel of Fig. 3, orange line. Simultaneously, a duration of the high performance phase of 2.5 s has been established. For a direct comparison, the W_{dia} time trace of the transient high performance program after pellet injections⁴ is shown with a dashed gray line in Fig. 3. As can be seen, Scenario 4 exactly reobtained the W_{dia} peak value but significantly extended the duration of the high performance phase.

The key to this long time high performance is the establishment and the control of a centrally peaked electron density profile, as shown in Fig. 4 on the right, orange line. With the start of pure NBI heating at $t \geq 1$ s, the central electron density (and also the line averaged n_e shown in Fig. 3, blue line in the right middle panel) steadily rises, yielding a centrally peaked n_e profile in the high performance phase in contrast to the flat n_e profile in the standard performance phase, see blue and orange lines in Fig. 4 on the right. Note that this pronounced central n_e peaking exclusively appears in NBI only heating phases and, therefore, does not show up in Scenario 1. However, a continued exclusive NBI heating would also result in a continued and uncontrolled rise of the central density, yielding a reduction of the plasma

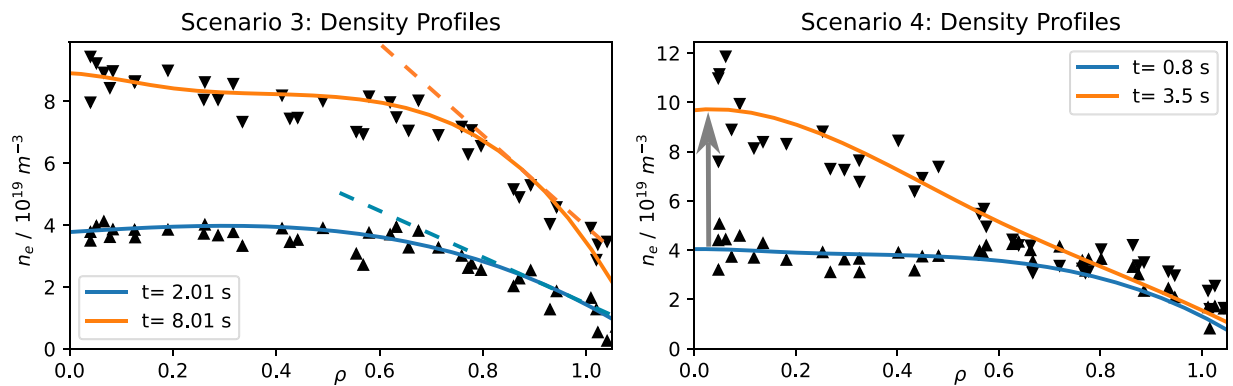


FIG. 4. Left: Electron density profiles for Scenario 3 in the standard (blue) and improved (orange) performance phases. Dashed lines indicate edge density gradients being higher in the case of improved performance. Right: Electron density profiles for Scenario 4 in the standard (blue) and improved (orange) performance phases.

TABLE I. Overview on the physics parameters of Scenarios 1–4. Important achievements of each scenario are highlighted.

Scenario	Scenario name	P_{ECRH}	P_{NBI}	HP duration	W_{dia}	τ_E	T_i	$n_e T_i \tau_E$
1	Steady NBI+ECRH	1.9 MW	3.0 MW	5.0 s	0.45 MJ	0.1 s	2.1 keV	$1.0 \times 10^{19} \text{ m}^{-3} \text{ keV s}$
2	Low edge density	1.6 MW	...	2.5 s	0.50 MJ	0.3 s	2.2 keV	$2.0 \times 10^{19} \text{ m}^{-3} \text{ keV s}$
3	Internal islands Configuration	4.0 MW	...	5.0 s	0.80 MJ	0.2 s	1.7 keV	$3.1 \times 10^{19} \text{ m}^{-3} \text{ keV s}$
4	Controlled density peaking	3.5 MW	4.1 MW	2.5 s	1.05 MJ	0.15 s	2.1 keV	$3.4 \times 10^{19} \text{ m}^{-3} \text{ keV s}$

temperature as the constant NBI heating power cannot compensate for the steadily increasing density level. In fact, this effect is already visible in the decreasing T_i during the pure NBI heating phase for $2 \leq t \leq 3$ s, see lower right panel of Fig. 3. The reintroduction of $P_{ECRH} = 2.5$ MW at $t = 3$ s has two positive effects: On the one hand, it stabilizes the peaked n_e profile at a central $n_e = 10 \times 10^{19} \text{ m}^{-3}$ and stops its further uncontrolled rise for $3 \leq t \leq 4$ s, see Fig. 3, middle right panel. On the other hand, the additional heating power brings up the plasma ion temperature above its saturation limit to $T_i = 2.0$ keV and yields the high W_{dia} .

Unfortunately, the control of the n_e profile peaking for NBI heated plasmas with ECRH is very sensitive to various actuators, *e.g.* the actual P_{ECRH} and P_{NBI} power levels, the initial electron density and others (to be discussed in detail elsewhere³⁵) making a feed forward control of these scenarios challenging. In particular toward the end of Scenario 4 at $t > 4$ s, the central n_e starts to rise again and a decrease in plasma T_i and W_{dia} occurs. For this case, a further adjustment of P_{ECRH} would be necessary, using, *e.g.*, a feedback control on the electron density. Strategies for feedback control of various actuators are currently under discussion and will be established and tested in the upcoming experimental campaigns of W7-X. It should be mentioned that Scenario 4 has also been performed successfully in other magnetic configurations like standard and high mirror³⁶ but with 5%–10% slightly reduced performance.

As evident from Figs. 2 and 4, any phase of improved performance is linked to an enhanced electron density gradient, either by its increase at the plasma edge (Scenarios 1 and 3) or by its increased radial extension (Scenarios 2 and 4). This empirical found correlation between increased density gradient and improved performance can be attributed to a reduction of turbulence, observed experimentally via reduced density fluctuation levels³⁷ and expected theoretically.¹⁰

III. PLASMA PERFORMANCE: ENERGY CONFINEMENT AND FUSION TRIPLE PRODUCT

For a quantitative analysis on the high performance phases of Scenarios 1–4, time traces of the two commonly used plasma parameters, energy confinement time τ_E and fusion triple product $n_e T_i \tau_E$, are shown in Fig. 5. In addition, the expected τ_E according to the ISS04 scaling is shown (dashed lines), being a benchmark of the empirical energy confinement scaling of various stellarator experiments with respect to several technical and physics machine parameters.¹⁹ In case τ_E meets the ISS04 scaling, the developed plasma scenario has an equally good performance as other stellarator experiments.

Figure 5 clearly shows the stationary character of the improved performance phases in Scenarios 1–4 in terms of both energy confinement and fusion triple product being constant for a duration of 3–5 s being 10–20 times the energy confinement time. As τ_E is defined as

$W_{dia}/P_{HEAT} + dW_{dia}/dt$, Scenarios 1 and 4 show a slight drop of τ_E and τ_{ISS04} when the NBI heating is switched on and off. Also evident from Fig. 5, Scenario 2 meets the ISS04 scaling for its entire high performance phase, and Scenarios 1, 3, and 4 achieve $\tau_E/\tau_{ISS04} = 0.8 - 0.9$. Both results are a reasonable improvement of the performance compared to standard gas fueled W7-X plasmas where τ_E does not exceed $\tau_E/\tau_{ISS04} \leq 0.7$ for $n_e > 5 \times 10^{19}$ and $\tau_E/\tau_{ISS04} \leq 0.9$ for $n_e < 5 \times 10^{19}$,²⁰ especially not for a duration on the order of seconds. For short transient phases of about 200 ms, τ_E/τ_{ISS04} could be exceeded over a value of 1.0 in previous campaigns^{3,4} exclusively in scenarios with pellet injections. For technical reasons, however, up until now, these scenarios and a possible extension of the HP phase could not be further developed.

The absolute values of the fusion triple products of Scenarios 1 and 2 are with $n_e T_i \tau_E \leq 2 \times 10^{19} \text{ m}^{-3} \cdot \text{keV} \cdot \text{s}$ comparably low due to the low electron density levels. With increased density and heating power however, the fusion product reaches $n_e T_i \tau_E = 3.5 \times 10^{19} \text{ m}^{-3} \cdot \text{keV} \cdot \text{s}$ in Scenarios 3 and 4 with a peak value of $n_e T_i \tau_E = 4.0 \times 10^{19} \text{ m}^{-3} \cdot \text{keV} \cdot \text{s}$ in Scenario 4. For comparison to previously observed transient high performance plasmas, the gray line in Fig. 5 shows the fusion product after pellet injections.⁴ Although the peak value of pellet fueled plasmas could not be met, the duration of improved performance could be increased by a factor of 10 and 5 in Scenarios 3 and 4, respectively.

IV. SUMMARY AND CONCLUSIONS

Table I summarizes the main physics parameters of Scenarios 1–4. Their main characteristics can be summarized as follows:

Scenario 1 is well suited to stationary overcome the T_i limit for up to 5 s, however, with limited performance regarding W_{dia} , τ_E , and $n_e T_i \tau_E$.

Scenario 2 shows a particular high energy confinement time of $\tau_E = 300$ ms, meeting the ISS04 scaling for a duration of 2.5 s. The scenario reproducibility and application for higher heating powers need further experimental investigation.

Scenario 3 is currently the best candidate for a long pulse, high performance program as it shows high performance regarding W_{dia} , τ_E , and $n_e T_i \tau_E$ and could be extended to a duration of several minutes, by simply extending the ECR heating phase. However, with the internal islands, its magnetic configuration does not properly cover the W7-X divertor and is, therefore, not reactor relevant due to its non-optimal pumping and exhaust capabilities.

Scenario 4 shows the highest performance of all four scenarios, in particular with respect to W_{dia} and $n_e T_i \tau_E$ but is currently tricky to stabilize and needs the development of a feedback control of the ECRH to be run in steady-state conditions.

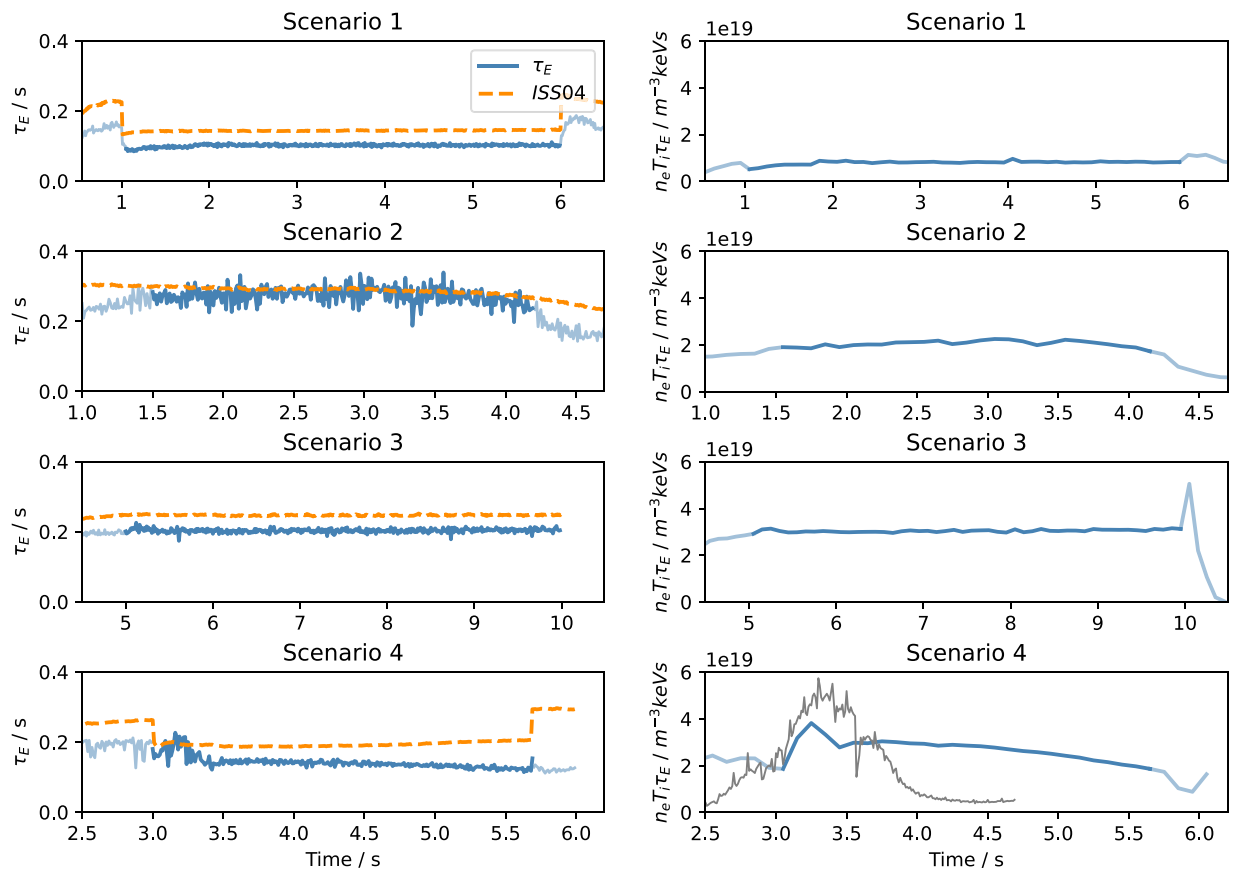


FIG. 5. Left: Time traces of energy confinement times (solid lines) with respect to the ISS04 scaling (dashed lines) for Scenarios 1–4. Right: Time traces of the fusion triple product for Scenarios 1–4. The thin gray solid line corresponds to the transient high performance scenario after pellet injections for comparison. Periods of improved performance are highlighted.

In summary, all four new developed scenarios clearly overcame one or more of the above-mentioned performance limitations for several seconds, being 10–20 times the energy confinement time. Therefore, the here developed scenarios are ideal candidates for a further improvement of the plasma performance and its duration. An important question to be answered in upcoming experiment campaigns is if stationary scenarios come at the cost of reduced performance, as is the case right now for, e.g., the fusion product. To answer this question, a twofold strategy, namely,

- experiments on the sustainment of high performance in pellet fueled plasmas through continuous pellet injections and
- performance optimization of HP scenarios through increased ECR and NBI heating powers,

will be followed that, based on the outcomes of this work, predict to yield promising results.

ACKNOWLEDGMENTS

This work has been carried out within the framework of the EUROfusion Consortium, funded by the European Union via the Euratom Research and Training Programme (Grant Agreement No.

101052200-EUROfusion). Views and opinions expressed are, however, those of the author(s) only and do not necessarily reflect those of the European Union or the European Commission. Neither the European Union nor the European Commission can be held responsible for them.

AUTHOR DECLARATIONS

Conflict of Interest

The authors have no conflicts to disclose.

Author Contributions

A. Langenberg: Conceptualization (lead); Data curation (lead); Formal analysis (lead); Writing – original draft (lead). **F. Warmer:** Writing – original draft (supporting). **G. Fuchert:** Conceptualization (equal); Formal analysis (supporting). **O. Ford:** Conceptualization (equal). **S. Bozhenkov:** Conceptualization (equal). **T. Andreeva:** Conceptualization (equal). **S. Lazerson:** Conceptualization (equal). **N. A. Pablant:** Data curation (supporting); Formal analysis (equal); Resources (supporting); Validation (supporting). **T. Gonda:** Formal analysis (supporting); Resources (supporting). **M. N. A. Beurskens:** Conceptualization (supporting). **K.-J. Brunner:** Formal analysis

(supporting). **B. Buttenschön:** Formal analysis (supporting). **A. Dinklage:** Conceptualization (supporting). **D. Hartmann:** Formal analysis (supporting). **J. Knauer:** Formal analysis (supporting). **O. Marchuk:** Validation (supporting); Writing – review & editing (supporting). **E. Pasch:** Formal analysis (supporting). **F. Reimold:** Conceptualization (supporting); Writing – review & editing (supporting). **T. Stange:** Conceptualization (supporting); Formal analysis (supporting). **Th. Wegner:** Formal analysis (supporting); Writing – review & editing (supporting). **O. Grulke:** Conceptualization (supporting); Supervision (supporting). **R. C. Wolf:** Supervision (lead); Writing – review & editing (supporting).

DATA AVAILABILITY

The data that support the findings of this study are available from the corresponding author upon reasonable request.

REFERENCES

- ¹X. L. Litaudon, H. S. Bosch, T. Morisaki, M. Barbarino, A. Bock, E. Belonohy, S. Brezinsek, J. B. Bucalossi, S. Coda, D. Raju, A. Ekedahl, K. Hanada, C. T. Holcomb, J. Huang, S. Ide, M. Jakubowski, B. V. Kuteev, E. A. Lerche, T. C. Luce, P. Maget, Y. Song, J. Stober, D. van Houtte, Y. K. Xi, L. Xue, S. W. Yoon, and B. Zhang, *Nucl. Fusion* **64**, 015001 (2023).
- ²R. C. Wolf, A. Alonso, S. Äkäslompolo, J. Baldzuhn, M. Beurskens, C. D. Beidler, C. Biedermann, H.-S. Bosch, S. Bozhrenkov, R. Brakel, H. Braune, S. Brezinsek, K.-J. Brunner, H. Damm, A. Dinklage, P. Drewelow, F. Effenberg, Y. Feng, O. Ford, G. Fuchert, Y. Gao, J. Geiger, O. Grulke, N. Harder, D. Hartmann, P. Helander, B. Heinemann, M. Hirsch, U. Höfel, C. Hopf, K. Ida, M. Isobe, M. W. Jakubowski, Y. O. Kazakov, C. Killer, T. Klinger, J. Knauer, R. König, M. Krychowiak, A. Langenberg, H. P. Laqua, S. Lazerson, P. McNeely, S. Marsen, N. Marushchenko, R. Nocentini, K. Ogawa, G. Orozco, M. Osakabe, M. Otte, N. Pablant, E. Pasch, A. Pavone, M. Porkolab, A. Puig Sitjes, K. Rahbarnia, R. Riedl, N. Rust, E. Scott, J. Schilling, R. Schroeder, T. Stange, A. von Stechow, E. Strumberger, T. Sunn Pedersen, J. Svensson, H. Thomson, Y. Turkin, L. Vano, T. Wauters, G. Wurden, M. Yoshinuma, M. Zanini, D. Zhang, and the Wendelstein 7-X Team, *Phys. Plasmas* **26**, 082504 (2019).
- ³C. D. Beidler, H. M. Smith, A. Alonso, T. Andreeva, J. Baldzuhn, M. N. A. Beurskens, M. Borchardt, S. A. Bozhrenkov, K. J. Brunner, H. Damm, M. Drevlak, O. P. Ford, J. Geiger, and P. Helander, *Nature* **596**, 221–226 (2021).
- ⁴S. A. Bozhrenkov, Y. Kazakov, O. Ford, M. N. A. Beurskens, J. A. Alcuson, J. A. Alonso, J. Baldzuhn, C. Brandt, K. J. Brunner, H. Damm *et al.*, *Nucl. Fusion* **60**, 066011 (2020).
- ⁵M. Krychowiak, R. König, T. Barbui, S. Brezinsek, J. Brunner, F. Effenberg, M. Endler, Y. Feng, E. Flom, Y. Gao, D. Gradic, P. Hacker, J. Harris, M. Hirsch, U. Höfel, M. Jakubowski, P. Kornejew, M. Otte, A. Pandey, T. Pedersen, A. Puig, F. Reimold, O. Schmitz, T. Schröder, V. Winters, and D. Zhang, *Nucl. Mater. Energy* **34**, 101363 (2023).
- ⁶D. Zhang, R. König, Y. Feng, R. Burhenn, S. Brezinsek, M. Jakubowski, B. Buttenschön, H. Niemann, A. Pavone, M. Krychowiak, S. Kwak, J. Svensson, Y. Gao, T. S. Pedersen, A. Alonso, J. Baldzuhn, C. D. Beidler, C. Biedermann, S. Bozhrenkov, K. J. Brunner, H. Damm, M. Hirsch, L. Giannone, P. Drewelow, F. Effenberg, G. Fuchert, K. C. Hammond, U. Höfel, C. Killer, J. Knauer, H. P. Laqua, R. Laube, N. Pablant, E. Pasch, F. Penzel, K. Rahbarnia, F. Reimold, H. Thomsen, V. Winters, F. Wagner, T. Klinger, and the W7-X Team, *Phys. Rev. Lett.* **123**, 025002 (2019).
- ⁷D. Carralero, T. Estrada, E. Maragkoudakis, T. Windisch, J. A. Alonso, J. L. Velasco, O. Ford, M. Jakubowski, S. Lazerson, M. Beurskens, S. Bozhrenkov, I. Calvo, H. Damm, G. Fuchert, J. M. Garcia-Regana, U. Höfel, N. Marushchenko, N. Pablant, E. Sanchez, H. M. Smith, E. Pasch, T. Stange, and the W7-X Team, *Plasma Phys. Controlled Fusion* **64**, 044006 (2022).
- ⁸T. S. Pedersen, I. Abramovic, P. Agostinetti, M. A. Torres, S. Äkäslompolo, J. A. Belloso, P. Aleynikov, K. Aleynikova, M. Alhashimi, A. Ali, N. Allen, A. Alonso, G. Anda *et al.*, *Nucl. Fusion* **62**, 042022 (2022).
- ⁹N. A. Pablant, A. Langenberg, J. A. Alonso, M. Bitter, S. A. Bozhrenkov, O. P. Ford, K. W. Hill, J. Kring, O. Marchuck, J. Svensson, P. Traverso, T. Windisch, Y. Yakusevitch, and the W7-X Team, *Rev. Sci. Instrum.* **92**, 043530 (2021).
- ¹⁰P. Xanthopoulos, S. A. Bozhrenkov, M. N. Beurskens, H. M. Smith, G. G. Plunk, P. Helander, C. D. Beidler, J. A. Alcuson, A. Alonso, A. Dinklage, O. Ford, G. Fuchert, J. Geiger, J. H. E. Proll, M. J. Poeschel, Y. Turkin, F. Warmer, and the W7-X Team, *Phys. Rev. Lett.* **125**, 075001 (2020).
- ¹¹T. Romba, F. Reimold, R. Jaspers, O. Ford, L. Vano, T. Klinger, and the W7-X Team, *Nucl. Fusion* **63**, 076023 (2023).
- ¹²T. Wegner, J.-P. Böhner, B. Buttenschön, A. Langenberg, A. von Stechow, and the W7-X Team, *J. Plasma Phys.* **89**, 955890302 (2023).
- ¹³J. M. García-Regaña, M. Barnes, I. Calvo, F. I. Parra, J. A. Alcuson, R. Davies, A. González-Jerez, A. Mollén, E. Sánchez, J. L. Velasco *et al.*, *J. Plasma Phys.* **87**, 855870103 (2021).
- ¹⁴A. Langenberg, T. Wegner, O. Marchuk, J. Garcia-Regana, N. Pablant, G. Fuchert, S. Bozhrenkov, H. Damm, E. Pasch, K.-J. Brunner, J. Knauer, M. Beurskens, F. Reimold, R. Wolf, and the W7-X Team, *Nucl. Fusion* **61**, 116018 (2021).
- ¹⁵A. Langenberg, T. Wegner, N. A. Pablant, O. Marchuk, B. Geiger, N. Tamura, R. Bussiahn, M. Kubkowska, A. Mollen, P. Traverso, H. M. Smith, G. Fuchert, S. Bozhrenkov, H. Damm, E. Pasch, K.-J. Brunner, J. Knauer, M. Beurskens, R. Burhenn, R. C. Wolf, and the W7-X Team, *Phys. Plasmas* **27**, 052510 (2020).
- ¹⁶T. Wegner, J. Alcuson, B. Geiger, A. V. Stechow, P. Xanthopoulos, C. Angioni, M. Beurskens, L.-G. Böttger, S. Bozhrenkov, K. Brunner, R. Burhenn, B. Buttenschön, H. Damm, E. Edlund, O. Ford, G. Fuchert, O. Grulke, Z. Huang, J. Knauer, F. Kunkel, A. Langenberg, N. Pablant, E. Pasch, K. Rahbarnia, J. Schilling, H. Thomsen, L. Vano, and the W7-X Team, *Nucl. Fusion* **60**, 124004 (2020).
- ¹⁷B. Geiger, T. Wegner, C. Beidler, R. Burhenn, B. Buttenschön, R. Dux, A. Langenberg, N. Pablant, T. Pütterich, Y. Turkin, T. Windisch, V. Winters, M. Beurskens, C. Biedermann, K. Brunner, G. Cseh, H. Damm, F. Effenberg, G. Fuchert, O. Grulke, J. Harris, C. Killer, J. Knauer, G. Kocsis, A. Krämer-Flecken, T. Kremeyer, M. Krychowiak, O. Marchuk, D. Nicolai, K. Rahbarnia, G. Satheeswaran, J. Schilling, O. Schmitz, T. Schröder, T. Szepesi, H. Thomsen, H. T. Mora, P. Traverso, D. Zhang, and the W7-X Team, *Nucl. Fusion* **59**, 046009 (2019).
- ¹⁸M. Beurskens, S. Bozhrenkov, O. Ford, P. Xanthopoulos, A. Zocco, Y. Turkin, A. Alonso, C. Beidler, I. Calvo, D. Carralero, T. Estrada, G. Fuchert, O. Grulke, M. Hirsch, K. Ida, M. Jakubowski, C. Killer, M. Krychowiak, S. Kwak, S. Lazerson, A. Langenberg, R. Lunsford, N. Pablant, E. Pasch, A. Pavone, F. Reimold, T. Romba, A. von Stechow, H. Smith, T. Windisch, M. Yoshinuma, D. Zhang, R. Wolf, and the W7-X Team, *Nucl. Fusion* **61**, 116072 (2021).
- ¹⁹H. Yamada, J. Harris, A. Dinklage, E. Ascasibar, F. Sano, S. Okamura, J. Talmadge, U. Stroth, A. Kus, S. Murakami, M. Yokoyama, C. Beidler, V. Tribaldos, K. Watanabe, and Y. Suzuki, *Nucl. Fusion* **45**, 1684 (2005).
- ²⁰G. Fuchert, K. Brunner, K. Rahbarnia, T. Stange, D. Zhang, J. Baldzuhn, S. Bozhrenkov, C. Beidler, M. Beurskens, S. Brezinsek, R. Burhenn, H. Damm, A. Dinklage, Y. Feng, P. Hacker, M. Hirsch, Y. Kazakov, J. Knauer, A. Langenberg, H. Laqua, S. Lazerson, N. Pablant, E. Pasch, F. Reimold, T. Pedersen, E. Scott, F. Warmer, V. Winters, and R. Wolf, *Nucl. Fusion* **60**, 036020 (2020).
- ²¹J. Baldzuhn, H. Damm, C. D. Beidler, K. McCarthy, N. Panadero, C. Biedermann, S. A. Bozhrenkov, A. Dinklage, K. J. Brunner, G. Fuchert, Y. Kazakov, M. Beurskens, M. Dibon, J. Geiger, O. Grulke, U. Höfel, T. Klinger, F. Köchl, J. Knauer, G. Kocsis, P. Kornejew, P. T. Lang, A. Langenberg, H. Laqua, N. A. Pablant, E. Pasch, T. S. Pedersen, B. Ploekel, K. Rahbarnia, G. Schlisio, E. R. Scott, T. Stange, A. V. Stechow, T. Szepesi, Y. Turkin, F. Wagner, V. Winters, G. Wurden, D. Zhang, and the Wendelstein 7-X Team, *Plasma Phys. Controlled Fusion* **62**, 055012 (2020).
- ²²S. A. Lazerson, O. Ford, S. Äkäslompolo, S. Bozhrenkov, C. Slaby, L. Vano, A. Spanier, P. McNeely, N. Rust, D. Hartmann, P. Poloskei, B. Buttenschön, R. Burhenn, N. Tamura, R. Bussiahn, T. Wegner, M. Drevlak, Y. Turkin, K. Ogawa, J. Knauer, K. J. Brunner, E. Pasch, M. Beurskens, H. Damm, G. Fuchert, P. Nelde, E. Scott, N. Pablant, A. Langenberg, P. Traverso, P. Valson, U. Hergenhan, A. Pavone, K. Rahbarnia, T. Andreeva, J. Schilling, C. Brandt, U. Neuner, H. Thomsen, N. Chaudhary, U. Höfel, T. Stange, G. Weir, N. Marushchenko, M. Jakubowski, A. Ali, Y. Gao, H. Niemann, A. P. Sitjes, R.

- König, R. Schroeder, N. den Harder, B. Heinemann, C. Hopf, R. Riedl, R. C. Wolf, and the W7-X Team, *Nucl. Fusion* **61**, 096008 (2021).
- ²³R. Lunsford, C. Killer, A. Nagy, D. A. Gates, T. Klinger, A. Dinklage, G. Satheeswaran, G. Kocsis, S. A. Lazerson, F. Nespoli, N. A. Pablant, A. von Stechow, A. Alonso, T. Andreeva, M. Beurskens, C. Biedermann, S. Brezinsek, K. J. Brunner, B. Buttenschön, D. Carralero, G. Cseh, P. Drewelow, F. Effenberg, T. Estrada, O. P. Ford, O. Grulke, U. Hergenbahn, U. Höfel, J. Knauer, M. Krause, M. Krychowiak, S. Kwak, A. Langenberg, U. Neuner, D. Nicolai, A. Pavone, A. Puig Sitjes, K. Rahbarnia, J. Schilling, J. Svensson, T. Szepesi, H. Thomsen, T. Wauters, T. Windisch, V. Winters, D. Zhang, L. Zsuga, and the W7-X Team, *Phys. Plasmas* **28**, 082506 (2021).
- ²⁴H. Laqua, J. Baldzuhn, H. Braune, S. Bozhnikov, K. Brunner, M. Hirsch, U. Höfel, J. Knauer, A. Langenberg, S. Marsen, D. Moseev, E. Pasch, K. Rahbarnia, T. Stange, R. Wolf, N. Pablant, O. Grulke, and the W7-X Team, *Nucl. Fusion* **61**, 106005 (2021).
- ²⁵S. Sereda, S. Brezinsek, E. Wang, T. Barbui, R. Brakel, B. Buttenschön, A. Gorjaev, U. Hergenbahn, U. Höfel, M. Jakubowski, A. Knieps, R. König, M. Krychowiak, S. Kwak, Y. Liang, D. Naujoks, A. Pavone, M. Rasinski, L. Rudischhauser, M. Slezcka, J. Svensson, H. Viebke, T. Wauters, Y. Wei, V. Winters, D. Zhang, and the W7-X Team, *Nucl. Fusion* **60**, 086007 (2020).
- ²⁶A. Gorjaev, T. Wauters, R. Brakel, S. Brezinsek, A. Dinklage, J. Fellingner, H. Grote, D. Moseev, S. Sereda, O. Volzke, and the W7-X Team, *Phys. Scr.* **2020**, 014063.
- ²⁷T. Andreeva, J. Geiger, A. Dinklage, G. Wurden, H. Thomsen, K. Rahbarnia, J. Schmitt, M. Hirsch, G. Fuchert, C. Nührenberg, A. Alonso, C. Beidler, M. Beurskens, S. Bozhnikov, R. Brakel, C. Brandt, V. Bykov, M. Grahl, O. Grulke, C. Killer, G. Kocsis, T. Klinger, A. Krämer-Flecken, S. Lazerson, M. Otte, N. Pablant, J. Schilling, T. Windisch, and the W7-X Team, *Nucl. Fusion* **62**, 026032 (2022).
- ²⁸A. Dinklage, C. Beidler, P. Helander, G. Fuchert, H. Maassberg, K. Rahbarnia, T. Sunn Pedersen, Y. Turkin *et al.*, *Nat. Phys.* **14**, 855 (2018).
- ²⁹K. Brunner, T. Akiyama, M. Hirsch, J. Knauer, P. Kornejew, B. Kursinski, H. Laqua, J. Meineke, H. T. Mora, and R. C. Wolf, *J. Instrumen.* **13**, P09002 (2018).
- ³⁰K. Rahbarnia, H. Thomsen, U. Neuner, J. Schilling, J. Geiger, G. Fuchert, T. Andreeva, M. Endler, D. Hathiramani, T. Bluhm, M. Zilker, B. Carvalho, A. Werner, and the Wendelstein 7-X Team, *Nucl. Fusion* **58**, 096010 (2018).
- ³¹A. Langenberg, N. A. Pablant, T. Wegner, P. Traverso, O. Marchuk, T. Bräuer, B. Geiger, G. Fuchert, S. Bozhnikov, E. Pasch, O. Grulke, F. Kunkel, C. Killer, D. Nicolai, G. Satheeswaran, K. P. Hollfeld, B. Schweer, T. Krings, P. Drews, G. Offermanns, A. Pavone, J. Svensson, J. A. Alonso, R. Burhenn, R. C. Wolf, and the W7-X Team, *Rev. Sci. Instrum.* **89**, 10G101 (2018).
- ³²E. Pasch, M. N. A. Beurskens, S. A. Bozhnikov, G. Fuchert, J. Knauer, R. C. Wolf, and the W7-X Team, *Rev. Sci. Instrum.* **87**, 11E729 (2016).
- ³³T. S. Pedersen, R. König, M. Jakubowski, M. Krychowiak, D. Gradic, C. Killer, H. Niemann, T. Szepesi, U. Wenzel, A. Ali *et al.*, *Nucl. Fusion* **59**, 096014 (2019).
- ³⁴T. Estrada, D. Carralero, T. Windisch, E. Sanchez, J. Garcia-Regana, J. Martinez-Fernandez, A. de la Pena, J. Velasco, J. Alonso, M. Beurskens, S. Bozhnikov, H. Damm, G. Fuchert, R. Kleiber, N. Pablant, E. Pasch, and the W7-X Team, *Nucl. Fusion* **61**, 046008 (2021).
- ³⁵O. P. Ford, M. Beurskens, S. Bozhnikov, S. Lazerson, and L. Vano, "Turbulence-reduced high-performance scenarios in Wendelstein 7-X" (submitted for publication).
- ³⁶T. Andreeva, "Vacuum magnetic configurations of Wendelstein 7-X," in *Tech. Rep. IPP III/270* (Max-Planck-Institut für Plasmaphysik, Garching, 2002).
- ³⁷A. V. Stechow, O. Grulke, T. Wegner, J. H. E. Proll, J. A. Alcuson, H. M. Smith, J. Baldzuhn, C. D. Beidler, M. N. A. Beurskens, S. A. Bozhnikov, E. Edlund, B. Geiger, Z. Huang, O. P. Ford, G. Fuchert, A. Langenberg, N. Pablant, E. Pasch, M. Porkolab, K. Rahbarnia, J. Schilling, E. R. Scott, H. Thomsen, L. Vano, G. Weir, and the W7-X Team, "Suppression of core turbulence by profile shaping in Wendelstein 7-X" (in press).